Int. J. Heat Mass Transfer. Vol. 29, No. 3, pp. 403–415, 1986
Printed in Great Britain

0017–9310/86 $3.00 + 0.00

Mass and heat transfer by natural convection in a vertical slot filled with porous medium

OSVAIR V. TREVISAN and ADRIAN BEJAN
Department of Mechanical Engineering and Materials Science, Duke University, Durham, NC 27706, U.S.A.

(*Received* 25 *February* 1985 *and in final form* 16 *September* 1985)

Abstract—This paper reports an analytical and numerical study of natural convection heat and mass transfer through a vertical porous layer subjected to uniform fluxes of heat and mass from the side. The flow is driven by the combined buoyancy effect due to temperature and concentration variations through the porous medium. The first part of the study contains an analytical Oseen-linearized solution for the boundary-layer regime and $Le = 1$, and a similarity solution for heat-transfer-driven flows ($n = 0$) and $Le > 1$. The second part of the study contains an extensive series of numerical experiments that validate the analytical results and provide heat and mass transfer data in the domain not covered by analysis. The numerical results cover the Rayleigh number range $20 \leqslant Ra \leqslant 10^5$, the buoyancy ratio range $-11 \leqslant n \leqslant 9$, the geometric aspect ratio range $1 \leqslant H/L \leqslant 4$ and the Lewis number range $0.03 \leqslant Le \leqslant 40$.

INTRODUCTION

THE PURPOSE of this report is to summarize a fundamental analytical and numerical study of heat and mass transfer by natural convection in a porous medium saturated with fluid. The special feature of this study is the focus on flows driven by conditions of uniform heat and mass flux imposed along the two vertical side walls of the porous layer. This set of conditions comes closest to simulating the boundary conditions for heat and mass transfer in insulation systems exposed to thermal radiation heating (e.g. the migration of moisture through double walls filled with fibrous or granular insulation).

Although as demonstrated by a number of recent monographs [1–3] the phenomenon of natural convection through porous media has received considerable attention, the bulk of the existing work has been devoted to pure natural convection heat transfer, not to phenomena driven by the combined buoyancy effect due to temperature and concentration variations through the porous medium. The necessary first step in elucidating the main features of the combined heat and mass transfer phenomenon addressed in this paper has just been reported in ref. [4], in which pure scaling arguments were used to identify and sort out the most basic scales that characterize the flow, temperature and concentration fields in the immediate vicinity of a single vertical surface imbedded in a porous medium of different temperature and concentration.

In connection with the combined heat and mass transfer natural convection phenomenon of ref. [4], considerably more important from a practical standpoint is the configuration sketched in Fig. 1, namely, the vertical porous layer of finite thickness L and finite height H. In the first phase of our work on this configuration [5], we modeled the two vertical side walls as impermeable surfaces with imposed constant temperature and concentration. We were able to show that numerical simulations of the phenomenon are in agreement with the results of the scale analysis conducted along the lines of ref. [4] for the single-surface configuration. However, due to the constant temperature and concentration imposed along the vertical boundaries, we were unable to develop closed-form analytical solutions for engineering heat and mass transfer calculations, to improve on the order-of-magnitude estimates produced by scale analysis.

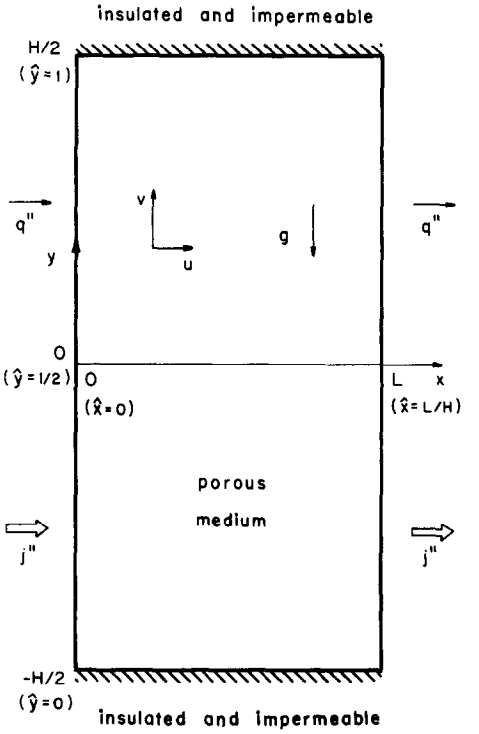

FIG. 1. Schematic of a two-dimensional porous layer subjected to uniform heat and mass fluxes in the horizontal direction.

NOMENCLATURE

- a core temperature gradient
- b core concentration gradient
- c concentration boundary-layer profile
- c_p specific heat at constant pressure
- C concentration
- ΔC average side-to-side concentration difference
- D mass diffusivity
- f similarity concentration profile
- g gravitational acceleration
- H height of porous layer
- j'' lateral mass flux
- k thermal conductivity
- K permeability
- L horizontal dimension (thickness) of porous layer
- Le Lewis number
- m number of control volumes in the vertical direction
- n buoyancy ratio, equation (18)
- Nu overall Nusselt number, equation (31)
- p number of control volumes in the horizontal direction
- q'' lateral heat flux
- Ra Rayleigh number, equation (34)
- s grid nonuniformity parameter (Fig. 2 and Table 2).
- Sh overall Sherwood number, equation (32)
- t temperature boundary-layer profile
- T temperature
- ΔT average side-to-side temperature difference
- u, v velocity components (Fig. 1)
- x, y Cartesian coordinates (Fig. 1)
- $\hat{x}$ horizontal position, $L-x$, Fig. 1
- $\hat{y}$ vertical position, equation (43).

Greek symbols

- α thermal diffusivity
- β thermal expansion coefficient
- β_C concentration expansion coefficient
- γ parameter, equation (17)
- λ constant, equation (41)
- η similarity variable
- ν kinematic viscosity
- ρ density
- Ψ streamfunction.

Subscripts and superscripts

- R properties of the right-side boundary-layer region, equations (24)–(26)
- 0 properties of the geometric center of the porous layer
- $\hat{}$ dimensionless variables, equation (47).

In the analytical and numerical work described in the present report the vertical side walls are assumed to be subjected to uniform fluxes of heat and mass, q'' and j''. This modelling decision is motivated first by the more frequent occurrence of practical conditions that approach the constant q'' and j'' description rather than the constant ΔT and ΔC model of ref. [5]; e.g. insulation layers exposed to radiation heating [6], and systems where the resistance to mass transfer through the side wall is greater than the mass transfer resistance contributed by the natural circulation process through the porous medium. The second reason for studying the constant q'' and j'' configuration of Fig. 1 is that with this new model it is possible to develop closed-form analytical solutions for overall heat and mass transfer calculations. Thus, one of the objectives of the numerical experiments summarized in this report is to validate and to show the range of applicability of the analytical results made possible by the constant q'', j'' model.

ANALYSIS OF THE BOUNDARY-LAYER REGIME

Consider the two-dimensional rectangular porous medium sketched in Fig. 1. The vertical walls are subjected to uniform fluxes of heat and mass,

$$q'' = -k\left(\frac{\partial T}{\partial x}\right)_{x=0,L}, \quad \text{constant} \tag{1}$$

$$j'' = -D\left(\frac{\partial C}{\partial x}\right)_{x=0,L}, \quad \text{constant} \tag{2}$$

while the horizontal walls are regarded as being insulated and impermeable. Note that according to Fig. 1, the boundary conditions (1) and (2) mean heating and mass influx at $x = 0$, and cooling combined with mass efflux at $x = L$. The equations governing the conservation of mass, momentum, energy and constituent in the solution-saturated porous medium are [1, 2]

$$\frac{\partial u}{\partial x} + \frac{\partial v}{\partial y} = 0 \tag{3}$$

$$\frac{\partial v}{\partial x} - \frac{\partial u}{\partial y} = \frac{gK}{\nu}\left(\beta\frac{\partial T}{\partial x} + \beta_C\frac{\partial C}{\partial x}\right) \tag{4}$$

$$u\frac{\partial T}{\partial x} + v\frac{\partial T}{\partial y} = \alpha\left(\frac{\partial^2 T}{\partial x^2} + \frac{\partial^2 T}{\partial y^2}\right) \tag{5}$$

$$u\frac{\partial C}{\partial x} + v\frac{\partial C}{\partial y} = D\left(\frac{\partial^2 C}{\partial x^2} + \frac{\partial^2 C}{\partial y^2}\right). \tag{6}$$

In writing the above equations, the porous medium has been modeled as homogeneous and with the solid and liquid phases in local thermal equilibrium. The solution that saturates the porous matrix is modeled as a Boussinesq-incompressible fluid whose density varies as $\rho = \rho_0[1-\beta(T-T_0)-\beta_C(C-C_0)]$ where β and β_C are the thermal and concentration expansion coefficients [4]. The other symbols appearing in equations (3)–(6) are defined in the Nomenclature and directly on Fig. 1.

In this section we present analyses of the boundary-layer regime, that is, of the regime where the fluid circulates through slender regions that line the two vertical walls in such a way that the thickness of each slender region is smaller than the horizontal extent of the porous layer, L (Fig. 1). According to the boundary-layer theory, the solution-saturated porous medium filling each boundary-layer region is governed by equations simpler than equations (4)–(6), namely [1, 2]

$$\frac{\partial v}{\partial x} = \frac{gK}{\nu}\left(\beta\frac{\partial T}{\partial x}+\beta_C\frac{\partial C}{\partial x}\right) \tag{7}$$

$$u\frac{\partial T}{\partial x}+v\frac{\partial T}{\partial y} = \alpha\frac{\partial^2 T}{\partial x^2} \tag{8}$$

$$u\frac{\partial C}{\partial x}+v\frac{\partial C}{\partial y} = D\frac{\partial^2 C}{\partial x^2}. \tag{9}$$

In what follows we outline two analytical solutions pertaining to the boundary layer regime: each solution applies in a certain range of values of the porous medium Lewis number $Le = \alpha/D$.

Oseen-linearized solution

It is possible to construct a matched boundary-layer solution for the constant q'' and j'' configuration of Fig. 1, by following the example presented in ref. [6] for the limiting problem in which the mass transfer from the side is absent. Summarizing the results of ref. [6], the main features of the matched boundary-layers solution for uniform heat flux from the side are: (1) constant, y-independent, boundary-layer thickness; (2) motionless core region ($u = 0$, $v = 0$); (3) linearly stratified core region; and (4) side-wall temperature that increases linearly with altitude at the same rate as the core temperature. These properties, in the context of the more general heat and mass transfer problem considered in this study, suggest the following transformation for the temperature and concentration fields in each vertical boundary-layer region,

$$T(x, y) = t(x)+T_0+ay \tag{10}$$

$$C(x, y) = c(x)+C_0+by \tag{11}$$

where the constants T_0 and C_0 are the temperature and concentration measured in the center of the porous layer ($x = L/2$, $y = 0$ on Fig. 1), and where a and b are the unknown constant vertical gradients of temperature and concentration measured through the core region. Functions $t(x)$ and $c(x)$ are the boundary-layer temperature and concentration profiles, respectively; in the left-side boundary-layer region on Fig. 1, these profiles have the property

$$\lim_{x\to\infty}(t, c) = 0. \tag{12}$$

Subjecting the boundary-layer equations (7)–(9) to the above transformation yields, in order,

$$v = \frac{Kg}{\nu}(\beta t+\beta_C c) \tag{13}$$

$$av = \alpha t'' \tag{14}$$

$$bv = Dc''. \tag{15}$$

The boundary-layer momentum equation (13) resulted from integrating equation (7) across the boundary layer and claiming the core limiting condition of equation (12). Eliminating v and c between equations (13)–(15) yields the fourth-order linear equation for $t(x)$,

$$t^{iv}-\gamma^2 t'' = 0 \tag{16}$$

$$\gamma^2 = \frac{Kg\beta a}{\alpha\nu}(1+n) \tag{17}$$

$$n = \frac{\alpha b\beta_C}{Da\beta} \tag{18}$$

whose general solution is

$$t(x) = A_1 e^{-\gamma x}+A_2 e^{\gamma x}+A_3+A_4 x. \tag{19}$$

Invoking the core condition (12) and the constant heat flux condition (1), the boundary-layer temperature profile (19) reduces to

$$t(x) = \frac{q''}{\gamma k}e^{-\gamma x} \tag{20}$$

The concentration profile $c(x)$ can be obtained by first dividing equations (14) and (15) side-by-side and integrating the resulting equation twice,

$$c(x) = \frac{\alpha b q''}{Dak\gamma}e^{-\gamma x}. \tag{21}$$

Applying the constant mass flux condition (2) to the concentration profile (21) yields an important relationship between the core stratification parameters a and b,

$$\frac{a}{b} = \frac{q''\alpha}{j''k}. \tag{22}$$

Finally, the vertical velocity profile compatible with results (20), (21) and equation (13) is

$$v = \frac{\alpha\gamma q''}{ak}e^{-\gamma x} \tag{23}$$

Summarizing the results developed so far, the boundary-layer region lining the left vertical wall in Fig. 1 is characterized by the velocity distribution (23), the temperature distribution (10) and (20), and the concentration distribution (11) and (21). Based on the centrosymmetry of the flow pattern we can write immediately the appropriate expressions for the right-

side of the porous layer,

$$T_R = -\frac{q''}{k\gamma} e^{-\gamma x_-} + T_0 + ay \tag{24}$$

$$c_R = -\frac{j''}{D\gamma} e^{-\gamma x_-} + C_0 + by \tag{25}$$

$$v_R = -\frac{\alpha\gamma q''}{ak} e^{-\gamma x_-} \tag{26}$$

where x_- is the horizontal coordinate measured in the negative x-direction away from the right wall ($x = L$). At this point the solution depends on the unknown core temperature and concentration gradients a and b. These constants can be determined by first recognizing that the net flow of enthalpy through the porous layer must at all ys be balanced by vertical thermal diffusion downward through the core [6],

$$\int_0^\infty \rho c_p v T \, dx + \int_0^\infty \rho c_p v_R T_R \, dx_- = \int_0^L k \frac{\partial T}{\partial y} dx \tag{27}$$

and, second, by writing the equivalent mass transfer condition (demanded by the zero mass flow through the top and bottom ends of the porous layer),

$$\int_0^\infty vC \, dx + \int_0^\infty v_R C_R \, dx_- = \int_0^L D \frac{\partial C}{\partial y} dx. \tag{28}$$

Conditions (27) and (28) yield, respectively,

$$a = \frac{q''}{k(\gamma L)^{1/2}} \tag{29}$$

$$b = \frac{j''}{D(\gamma L)^{1/2}}. \tag{30}$$

An important limitation of the analytical solution concluded above is determined by substituting the newly derived core gradients (a, b) into condition (22): the result is $Le = 1$, i.e. the Oseen-linearized solution is valid only for solution-saturated porous media in which the thermal diffusivity is the same as the mass diffusivity of constituent.

The heat and mass transfer engineering contribution of the solution reported above is the following set of analytical expressions for overall Nusselt and Sherwood numbers,

$$Nu = \frac{q''}{k\Delta T/L} = \frac{1}{2}\gamma L \tag{31}$$

$$Sh = \frac{j''}{D\Delta C/L} = \frac{1}{2}\gamma L \tag{32}$$

where ΔT and ΔC are the side-to-side temperature difference and concentration difference. Recalling the original γ notation, equation (17), and the result obtained for a, equation (29), the Nu and Sh expressions can be rewritten as

$$Nu = Sh = \frac{1}{2}\left(\frac{H}{L}\right)^{-4/5} Ra^{2/5}(1+n)^{2/5} \tag{33}$$

where Ra is the Rayleigh number based on uniform heat flux

$$Ra = \frac{Kg\beta H^2 q''}{\alpha\nu k}. \tag{34}$$

The analytical results culminating with equation (33) are valid provided the thermal and concentration boundary layers are distinct (i.e. thinner than L). Since the Nu and Sh definitions (31) and (32) are based on the pure diffusion estimates, the distinct-boundary-layers requirement translates into the condition $(Nu, Sh) > 1$, or $(L/H)Ra^{1/2}(1+n)^{1/2} > O(1)$.

One final observation concerns the sign of $(1+n)$, which was assumed positive in equation (17). The heat and mass transfer solution obtained for positive $(1+n)$ values holds also for negative values if in equation (33) the term $(1+n)$ is replaced by $|1+n|$. In order to see the generality of equation (33), consider that the momentum equation (7) can be rewritten as:

$$\frac{\partial v}{\partial x} = \pm|1+n|\frac{Kg\beta}{\nu}\frac{\partial T}{\partial x}. \tag{7'}$$

Since $\partial T/\partial x$ does not change sign (q'' is imposed, as shown in Fig. 1), the change in the sign of $(1+n)$ has the effect of changing the sign of v, i.e. that of reversing the flow. Equation (33) with $(1+n)$ replaced by $|1+n|$, is supported by the numerical results discussed later in this paper.

Similarity solution for $\mathrm{Le} \gg 1$ *and* $|n| \ll 1$

The effect of Lewis number on the mass transfer rate can be determined analytically by focusing on the so-called 'heat-transfer-driven flow' limit [4] where parameter n is in absolute value considerably smaller than one. In this limit the velocity and temperature fields are the ones reported already for the pure heat transfer problem [6]. If we now consider the mass transfer effected by this heat-transfer-driven flow, we must solve the constituent conservation equation (9) with $u = 0$ and v given by equation (23) with $n = 0$. In the limit of large Lewis numbers, the concentration boundary-layer region in which equation (9) is to be solved is much thinner than the velocity boundary-layer region. Consequently, in place of v in equation (9) we can use $v(x)$ evaluated at $x = 0$, and the constituent conservation equation reduces to

$$v(0)\frac{\partial C}{\partial y} = D\frac{\partial^2 C}{\partial x^2}. \tag{35}$$

This equation can be solved via similarity formulation subject to the condition of uniform mass flux from the side, equation (2), and that of a constant average concentration core filling the porous medium situated outside the concentration boundary layer. Omitting the algebra, the similarity formulation of the mass transfer problem is

$$f'' + \frac{\eta}{2}f' - \frac{1}{2}f = 0 \tag{36}$$

$$f' = -1 \quad \text{at} \quad \eta = 0 \tag{37}$$

$$f \to 0 \quad \text{as} \quad \eta \to \infty \tag{38}$$

where

$$C - C_0 = \left(\frac{\lambda}{Le}\hat{y}\right)^{1/2} f(\eta)\frac{j''}{D} HRa^{-1/3} \tag{39}$$

$$\eta = x_* \left(\frac{\lambda}{Le}\hat{y}\right)^{-1/2} \tag{40}$$

$$\lambda = \left(\frac{H}{L}\right)^{1/5} Ra^{1/15}, \quad \text{const [6]} \tag{41}$$

$$x_* = \frac{x}{H\,Ra^{-1/3}} \tag{42}$$

$$\hat{y} = \frac{y}{H} + \frac{1}{2}, \quad \text{Fig. 1.} \tag{43}$$

The problem stated in equations (36)–(43) was solved numerically using a fourth-order Runge–Kutta scheme and integrating equation (36) from $\eta = 0$ to η values of 10 or greater in accordance with the standard shooting method. The numerical solution reported in Table 1 was obtained using the shooting success criterion $f < 10^{-4}$ in place of the boundary condition (38). The $\Delta\eta$ step used to perform the integration was 0.001; this step size was found to be small enough to render the solution insensitive to further decreases in the step size.

The mass transfer result contained in the similarity solution of Table 1 can be reported as the overall Sherwood number

$$Sh = \frac{j''}{D\Delta C/L} = 0.665\left(\frac{L}{H}\right)^{11/10} Le^{1/2}Ra^{3/10} \tag{44}$$

where ΔC is the H-averaged concentration difference between the two sides of the porous layer,

$$\Delta C = \frac{2}{H}\int_{-H/2}^{H/2} (C - C_0)_{x=0}\,dy \tag{45}$$

with the difference $C - C_0$ being given by equation (39). The factor 2 appearing on the RHS of equation (45) accounts for the fact that the average side-to-side concentration difference is twice the average concentration difference across a single boundary layer.

Table 1. Similarity concentration profile for heat-transfer-driven flows and large Lewis numbers

η	f	f'
0.0	1.128	−1.000
0.5	0.698	−0.724
1.0	0.399	−0.479
1.5	0.209	−0.289
2.0	0.100	−0.157
2.5	0.044	−0.077
3.0	0.017	−0.034
3.5	0.006	−0.013
4.0	0.002	−0.005
4.5	0.001	−0.001
5.0	0.000	0.000

Finally, the overall Sherwood number formula (44) applies as long as the thermal and velocity boundary layers are distinct. Since the thickness of these layers scales as $HRa^{-2/5}(H/L)^{-1/5}$, ref. [6], the validity condition for the Sherwood number result (44) becomes

$$Ra^{1/2} > \frac{H}{L}. \tag{46}$$

If the thermal boundary layers are distinct, then the requirement of distinct concentration boundary layers is automatically satisfied since the Lewis number was assumed greater than one.

NUMERICAL ANALYSIS

The complete governing equations (3)–(6) were solved via finite differences in order to establish the validity of the analytical results developed in the first part of this study, and to furnish engineering heat and mass transfer data in the parametric domains not covered by analysis. The dimensionless formulation of the problem solved on the computer was:

Variables

$$\hat{x} = x/H, \quad \hat{y} = (y + H/2)/H$$

$$\hat{\Psi} = \frac{\Psi}{\alpha Ra}; \quad \text{where} \quad u = \partial\Psi/\partial y, \quad v = -\partial\Psi/\partial x$$

$$\hat{T} = \frac{T - T_0}{q''H/k}, \quad \hat{C} = \frac{C - C_0}{j''H/D} \tag{47}$$

Equations

$$\frac{\partial}{\partial\hat{x}}(\hat{T} + n\hat{C}) = -\nabla^2\hat{\Psi} \tag{48}$$

$$Ra\left(\frac{\partial\hat{\Psi}}{\partial\hat{y}}\frac{\partial\hat{T}}{\partial\hat{x}} - \frac{\partial\hat{\Psi}}{\partial\hat{x}}\frac{\partial\hat{T}}{\partial\hat{y}}\right) = \nabla^2\hat{T} \tag{49}$$

$$Le\,Ra\left(\frac{\partial\hat{\Psi}}{\partial\hat{y}}\frac{\partial\hat{C}}{\partial\hat{x}} - \frac{\partial\hat{\Psi}}{\partial\hat{x}}\frac{\partial\hat{C}}{\partial\hat{y}}\right) = \nabla^2\hat{C} \tag{50}$$

Boundary conditions

$$\hat{\Psi} = 0, \quad \frac{\partial\hat{T}}{\partial\hat{x}} = \frac{\partial\hat{C}}{\partial\hat{x}} = -1, \quad \text{at} \quad \hat{x} = 0, \quad L/H \tag{51}$$

$$\hat{\Psi} = 0, \quad \frac{\partial\hat{T}}{\partial\hat{y}} = \frac{\partial\hat{C}}{\partial\hat{y}} = 0, \quad \text{at} \quad \hat{y} = 0, 1 \tag{52}$$

where $\nabla^2 = \partial^2/\partial\hat{x}^2 + \partial^2/\partial\hat{y}^2$, and where parameters n, Ra and Le are the groups identified already in the analysis of the boundary-layer regime.

The numerical method consisted of approximating equation (48)–(50) using the control volume approach developed by Patankar [7]. The fluxes of heat and mass through the boundary of each control volume were calculated using the power law scheme. An iterative point-by-point method was used to solve the discretized equations, and the convergence of the

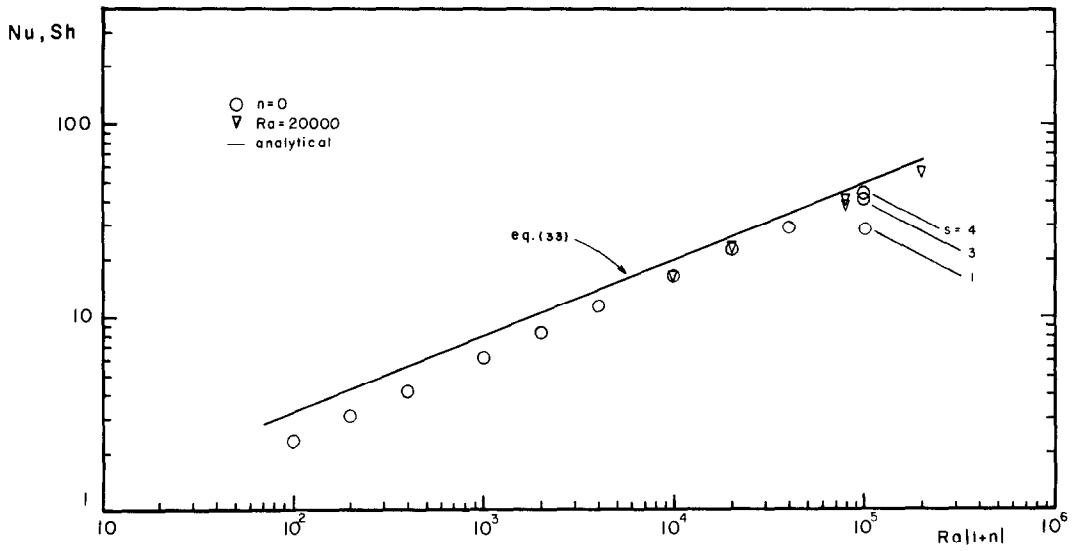

FIG. 2. Overall heat and mass transfer calculations showing the validity of the Oseen-linearized analysis and the effect of the grid nonuniformity parameter s.

solution was defined based on the criterion

$$\left.\begin{array}{l}\sum_{i,j}|\tau_{K+1}-\tau_K| \\ \sum_{i,j}|\tau_{K+1}|\end{array}\right\} < \text{Res} \qquad (53)$$

where τ stands for $\hat{\Psi}$, $\hat{T}$ or $\hat{C}$, and the subscript K indicates the iteration order. In most cases the residue, Res, was set equal to 10^{-5} so that the difference between two successive estimates of the diffusion-referenced overall Nusselt and Sherwood numbers defined below was less than 1%,

$$Nu = \frac{L}{H}\left(\int_0^1 \Delta\hat{T}\,d\hat{y}\right)^{-1} \qquad (54)$$

$$Sh = \frac{L}{H}\left(\int_0^1 \Delta\hat{C}\,d\hat{y}\right)^{-1} \qquad (55)$$

The two-dimensional domain of Fig. 1 was covered with a grid of $(m-1)\times(p-1)$ lines defining $m\times p$ control volumes. The grid was nonuniform: the control volumes situated near the boundaries were made sufficiently small so that in all cases at least three control volumes were situated inside the narrowest boundary-layer region. The effect of grid nonuniformity on accuracy is illustrated in Fig. 2 and Table 2 for the case of pure heat transfer in a square domain at a very high Rayleigh number ($Ra = 10^5, n = 0, Le = 1, H/L = 1$). Parameter s listed next to the points aligned vertically above the abscissa value of 10^5, represents the number of thinner control volumes generated by the divisions (cuts) made into a control volume situated next to the boundary. In the three cases aligned vertically above the abscissa point 10^5 in Fig. 2 the total number of control volumes in one direction (e.g. horizontal) is fixed at $p = 32$. The grid was built in such a way that the width of a thin control volume is $1/s$ of the width of one of the interior control volumes. In order to maintain the total number of control volumes constant ($p = 32$), the remaining space (the core) is covered by a decreasing number of control volumes of equal size. Relative to using a uniform grid, the use of the present nonuniform grid was found to accelerate the convergence of the solution.

Throughout the numerical part of this study the grid fineness used for square-shaped domains was 32×32. In tall domains, $H/L > 1$, the number of control volumes in the vertical direction was increased up to $m = 56$ (see Table 4); the number m was such that $(m-2s)/(p-2s)$ was equal to the geometric ratio H/L. The choice of a grid fineness such as 32×32 for

Table 2. Numerical results for heat-transfer-driven flows ($n = 0$), in a square box ($H/L = 1$) at $Le = 1$ (grid fineness 32×32)

Ra	s	Nu, Sh	$\hat{\Psi}_{min}$ ($\times 10^{-3}$)	$\Delta\hat{T}, \Delta\hat{C}$ ($\hat{y} = 0, 1$)	$\Delta\hat{T}, \Delta\hat{C}$ ($\hat{y} = 1/2$)
20	1	1.29	−51.6	0.802	0.747
40	1	1.61	−37.5	0.669	0.580
100	1	2.29	−21.8	0.503	0.387
200	1	3.06	−13.7	0.398	0.281
400	1	4.12	−8.3	0.312	0.205
1000	1	6.15	−4.2	0.221	0.136
2000	1	8.34	−2.5	0.166	0.101
4000	1	11.26	−1.5	0.122	0.076
10,000	1	16.36	−0.9	0.079	0.055
20,000	1	20.82	−0.6	0.057	0.045
	2	22.07	−0.5	0.063	0.040
40,000	1	24.88	−0.5	0.044	0.039
	2	28.85	−0.3	0.045	0.032
100,000	1	28.12	−0.4	0.037	0.035
	3	40.80	−0.2	0.030	0.023
	4	42.58	−0.1	0.032	0.021

$H/L = 1$ is based on the extensive grid fineness test reported in ref. [5].

The particular sets of (Ra, n, Le, H/L) values chosen for numerical analysis were organized in order to investigate systematically the effect of each dimensionless parameter and, ultimately, the validity of the analytical results reported in the preceding section.

A set of representative patterns of streamlines, isotherms and constant concentration lines is assembled in Figs. 3(a)–(d). The flow illustrated in Fig. 3(a) is heat-transfer-driven ($n = 0$) at high enough Rayleigh number so that the vertical boundary layers are distinct. The isotherms plotted in Fig. 3(b) confirm the main assumptions made in setting up the Oseen-linearized analysis, namely, the thermal boundary layers are of relatively constant thickness, and the core region is thermally stratified (the core temperature is mainly a function of altitude).

The concentration field that rides on the heat-transfer-driven flow depends to a significant degree on the Lewis number. This dependence is illustrated in Figs. 3(b)–(d) where the Lewis number assumes, in order, the values 1, 0.1 and 10 [note that the isotherms of Fig. 3(b) are the same as the constant concentration lines when $Le = 1$]. At small Lewis numbers [$Le = 0.1$, Fig. 3(c)], the concentration boundary layers are no longer distinct and the mass transfer through the porous layer is mainly by diffusion in the horizontal

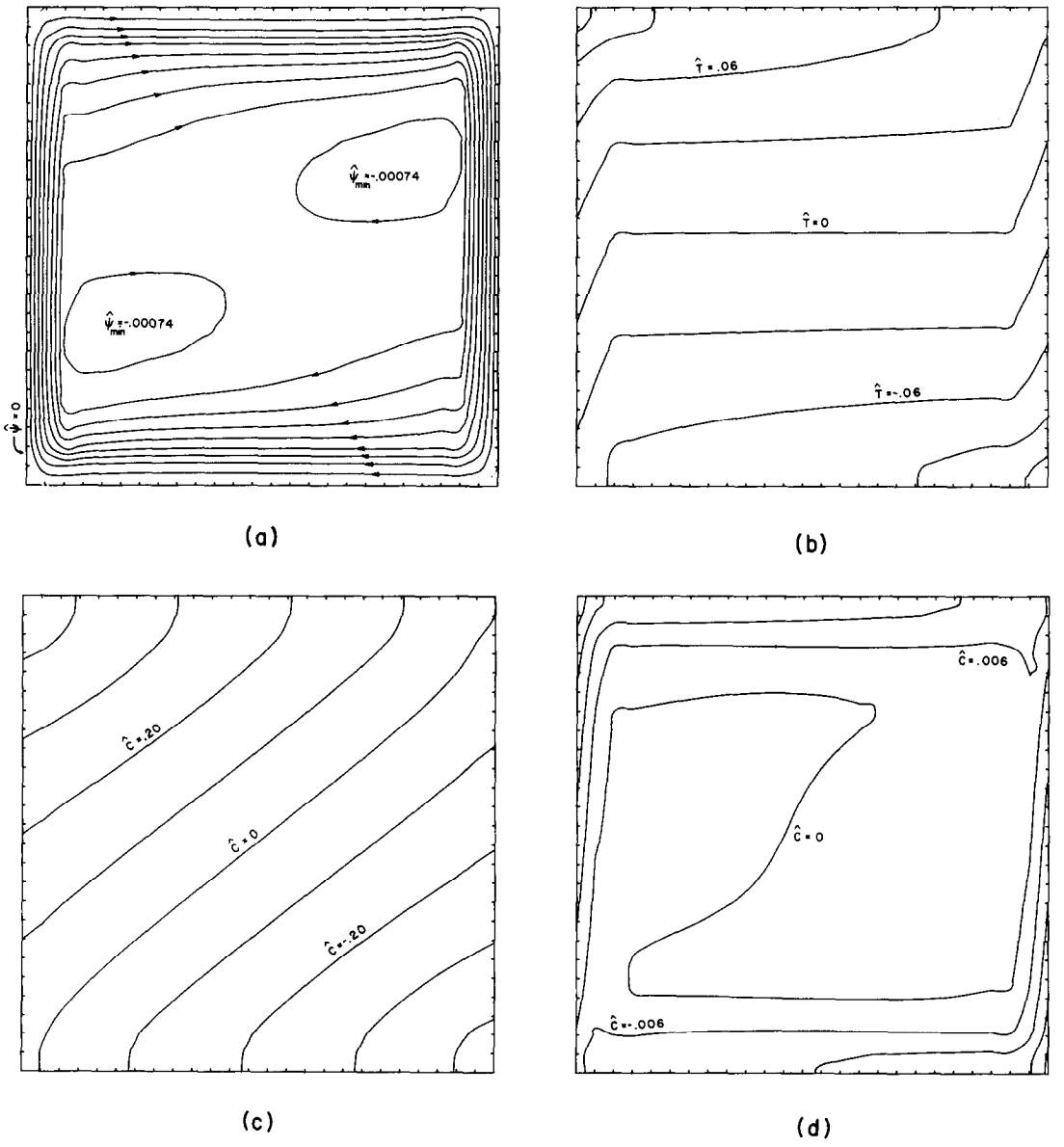

FIG. 3. Example of numerical solution for the flow, temperature and concentration fields ($n = 0$, $Ra = 10^4$, $H/L = 1$): (a) streamlines; (b) isotherms (or constant concentration lines when $Le = 1$); (c) constant concentration lines when $Le = 0.1$; (d) constant concentration lines when $Le = 10$.

Table 3. Numerical results showing the effect of varying the buoyancy ratio n in a square domain in the boundary-layer regime ($Ra = 2 \times 10^4$, $H/L = 1$, $Le = 1$, grid fineness 32×32)

n	s	Nu, Sh	$\hat{\Psi}_{max}$ ($\times 10^{-4}$)	$\hat{\Psi}_{min}$ ($\times 10^{-4}$)	$\Delta\hat{T}, \Delta\hat{C}$ ($\hat{y} = 0, 1$)	$\Delta\hat{T}, \Delta\hat{C}$ ($\hat{y} = 1/2$)
−11	4	54.84	8.8	0	0.023	0.017
−5	3	38.92	6.8	0	0.034	0.024
−3	2	29.46	5.8	0	0.045	0.031
−2	1	20.82	5.6	0	0.057	0.045
−1	1	1.01	0	0	0.993	0.993
0	2	22.07	0	−5.0	0.063	0.040
1	2	29.46	0	−5.8	0.045	0.031
3	2	37.45	0	−7.8	0.032	0.025
9	4	54.84	0	−8.8	0.023	0.017

direction. The opposite effect is encountered at high Lewis numbers [$Le = 10$, Fig. 3(d)], where the concentration boundary layers become sharper than the thermal boundary layers. In addition, at high Lewis numbers the mass diffusivity is low enough relative to the thermal diffusivity so that the horizontal instrusion layers lining the top and bottom walls are considerably sharper than their thermal counterparts [Fig. 3(b)]: the net result is that the core of the concentration field at high Lewis numbers is in a state of almost uniform concentration.

The Oseen-linearized solution that was concluded by the heat and mass transfer correlations (33) is tested quantitatively through the numerical experiments summarized in Tables 2–4 and Figs. 2, 4 and 5. In addition to the effect of the grid nonuniformity parameter s, discussed already, Fig. 2 presents a comparison between the heat and mass transfer data of Tables 2 and 3 and the analytical Nu, Sh result (33). The numerical data correspond to high Rayleigh number flows in porous media of square shape and Lewis number equal to one; the data belong to both heat-transfer-driven flows ($n = 0$, Table 2) and mass-transfer-driven flows (Table 3). On the log–log plot of Fig. 2, the data follow very closely the $(Ra|1+n|)^{1/5}$ trend anticipated theoretically, equation (33). The numerical results approach the theoretical line as the boundary-layer features become more pronounced, i.e. as the abscissa parameter increases.

Figure 4 tests one of the details of the Oseen-linearized solution, namely the exponential-decay temperature profiles in the boundary-layer region, equation (20). Shown in Fig. 4 are numerically calculated temperature profiles at $\hat{y} = 1/2$ for two different mass-transfer-driven flows ($n = 1, 9$): these calculations agree very well with the theoretical curves. Furthermore, as shown in Fig. 3(a), the thickness of the boundary-layer region is nearly constant: this feature was used as one of the basic assumptions in setting up the Oseen-linearized analysis.

The effect of increasing the geometric aspect ratio H/L is documented in Table 4 and projected on Fig. 5. The agreement between numerical results and equation (33) improves as the slenderness ratio H/L increases. This trend is consistent with the parallel boundary-layer structure of the flow assumption on which equation (33) is based. The validity of this assumption improves steadily as the porous medium becomes taller, provided the boundary layers are thin enough to remain distinct. This trend is also consistent with the fact that the agreement between the local mid-height numerical results and equation (33) is better than the agreement between the overall numerical results and equation (33).

Turning our attention now to the similarity solution that led to equation (44), Tables 5 and 6 summarize the numerical results obtained for porous media with Lewis numbers other than unity. All the flows considered in this series of numerical experiments are heat-transfer-driven ($n = 0$), in accordance with the main assumption used in constructing the similarity solution. The numerical data of Tables 5 and 6 are displayed in Figs. 6 and 7. In Fig. 6, all the numerical Sherwood number data for $Le \geqslant 1$ are used to test the validity of equation (44). Although the numerical calculations fall consistently above the analytical prediction based on equation (44), the $Sh \sim Le^{1/2}Ra^{3/10}$ scaling law anticipated theoretically is confirmed by numerical experiments.

Figure 7 illustrates the effect of Lewis number on the overall mass transfer rate in a square domain where the flow is of the boundary-layer type and is driven by buoyancy due to temperature variations ($n = 0$). As suggested earlier by the shift from Fig. 3(b) to (c), when

Table 4. Numerical results for mass-transfer-driven flows ($n = 3$) in a relatively tall domain ($Le = 1$, $p = 32$)

Aspect ratio	Ra	m/s	Nu, Sh	$\hat{\Psi}_{min}$ ($\times 10^{-4}$)	$\Delta\hat{T}, \Delta\hat{C}$ ($\hat{y} = 0, 1$)	$\Delta\hat{T}, \Delta\hat{C}$ ($\hat{y} = 1/2$)
$H/L = 2$	5000	44/4	13.48	−13.0	0.0597	0.0336
	10,000	44/4	17.85	−8.0	0.0444	0.0258
	20,000	44/4	23.44	−5.0	0.0325	0.0199
	40,000	44/4	30.48	−3.0	0.0234	0.0156
$H/L = 4$	10,000	56/4	10.52	−5.7	0.0380	0.0225
	20,000	56/4	13.82	−3.5	0.0283	0.0173
	40,000	56/4	17.73	−2.0	0.0216	0.0130
	100,000	48/8	22.72	−1.3	0.0144	0.0108

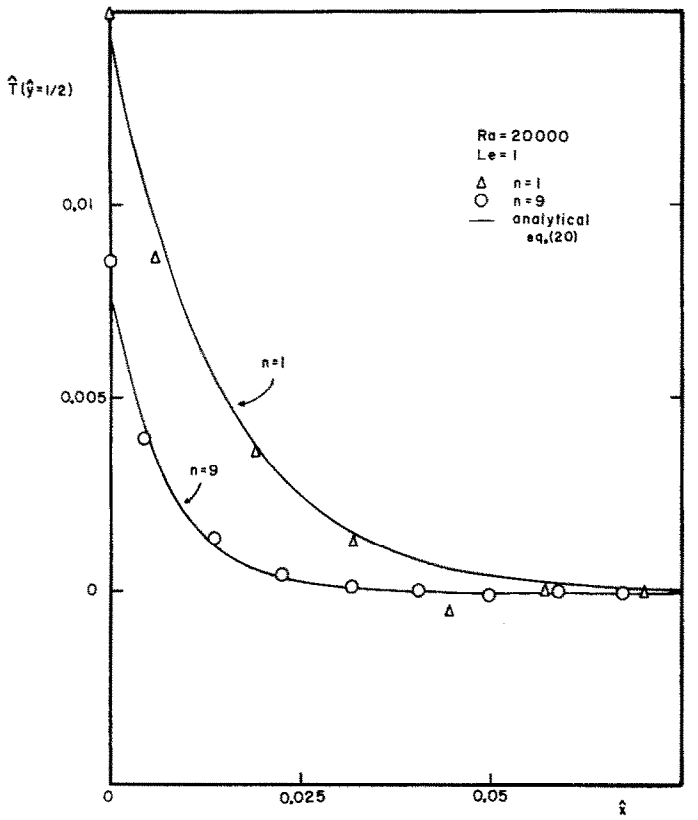

FIG. 4. The temperature distribution in the vertical boundary-layer region, showing a comparison between the Oseen-linearized solution and numerical calculations.

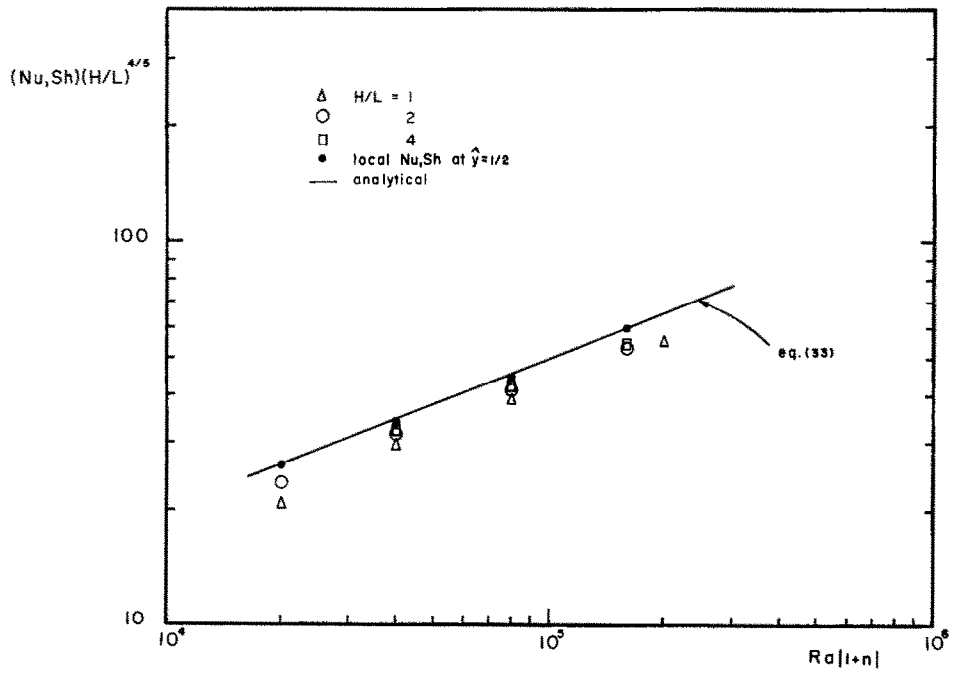

FIG. 5. Overall heat and mass transfer results in tall layers, showing the validity of the Oseen-linearized solution.

Table 5. Numerical results for heat-transfer-driven flows with $Le \neq 1$, showing the effect of increasing the Rayleigh number ($n = 0$, $H/L = 1$, grid fineness 32×32)

Ra	s	Nu	Sh $Le = 0.1$	$Le = 10$
20	1	1.29	1.00	6.06
40	1	1.61	1.01	7.89
100	1	2.29	1.02	10.89
200	1	3.06	1.03	13.59
400	1	4.12	1.05	16.66
1000	1	6.15	1.09	20.92
	3	6.12	—	24.03
2000	1	8.34	1.14	23.95
	2	8.28	—	29.05
4000	1	11.26	1.23	26.48
	2	11.20	—	34.67
10,000	1	16.36	1.50	28.73
	4	16.55	—	50.71
20,000	1	20.82	2.00	
40,000	1	24.88	3.23	

Table 6. Numerical results showing the response of mass transfer to varying the Lewis number ($n = 0$, $H/L = 1$, grid fineness 32×32)

Ra	Le	s	Nu	Sh
1000	0.03	1	6.15	1.00
	0.3	1	6.15	1.76
	2	2	6.13	11.05
	4	3	6.12	15.95
	20	4	6.12	33.23
	40	5	6.12	45.44
10,000	4	4	16.63	36.06
	40	8*	16.37	98.58

*In this case the grid was refined to 42×42

the Lewis number is small enough so that the concentration boundary-layer thickness becomes of order L, the side-to-side mass transfer process is ruled by pure diffusion and Sh becomes of order one. At the other end of the Le spectrum, where the concentration boundary layers are even more distinct than the thermal boundary layers, the Sherwood number scales as $Le^{1/2}$ in accordance with the similarity solution responsible for equation (44).

THE DOMAIN COVERED BY THE PRESENT STUDY

Figure 8 presents in three dimensions the domain occupied by the combined heat and mass transfer phenomenon investigated in this study. Shown in the same figure are the two limiting planes in which the two analytical solutions apply. With Fig. 8 in mind, reviewing the numerical data summarized in Tables 2–6 it is easy to see that the numerical experiments summarized in the second part of this study verify the validity of the two limiting analyses and, in addition, bridge the gaps between the two analytical solutions. Finally, it is worth keeping in mind that theoretically the parametric domain of Fig. 8 is known not only in the two limiting (boundary-layer regime) planes highlighted in this study, but also in the low Rayleigh number limit where the heat and mass transfer phenomenon is ruled by pure diffusion. To delineate the transition from the pure diffusion regime to the boundary-layer regime is the object of the 'distinct boundary-layer' criteria discussed in connection with equations (33) and (46).

Comparing the theoretical and numerical results of the present study with the numerical results of ref. [5] we are in a position to evaluate the effect of boundary conditions on engineering results such as the overall heat and mass transfer rates. In Fig. 9 we show overall

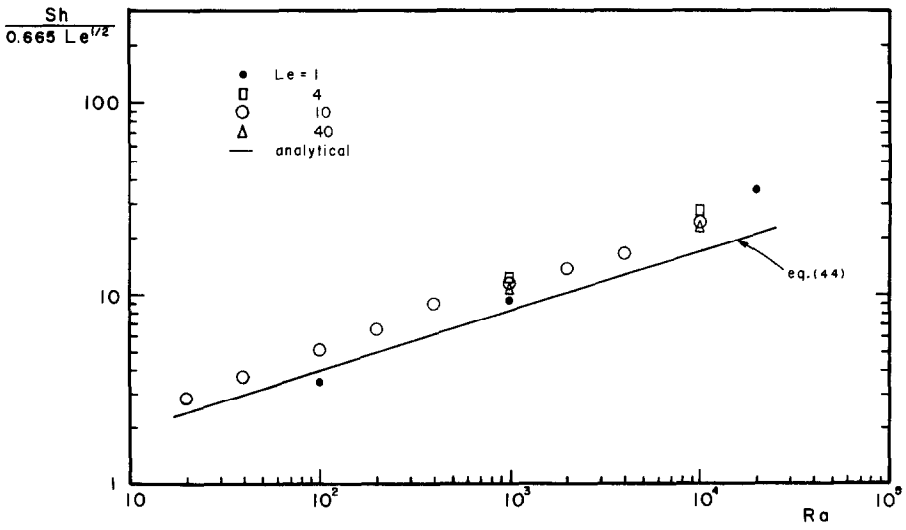

FIG. 6. The effect of Lewis number on mass transfer in heat transfer driven flows ($n = 0$, $H/L = 1$), and the validity of the similarity solution, equation (44).

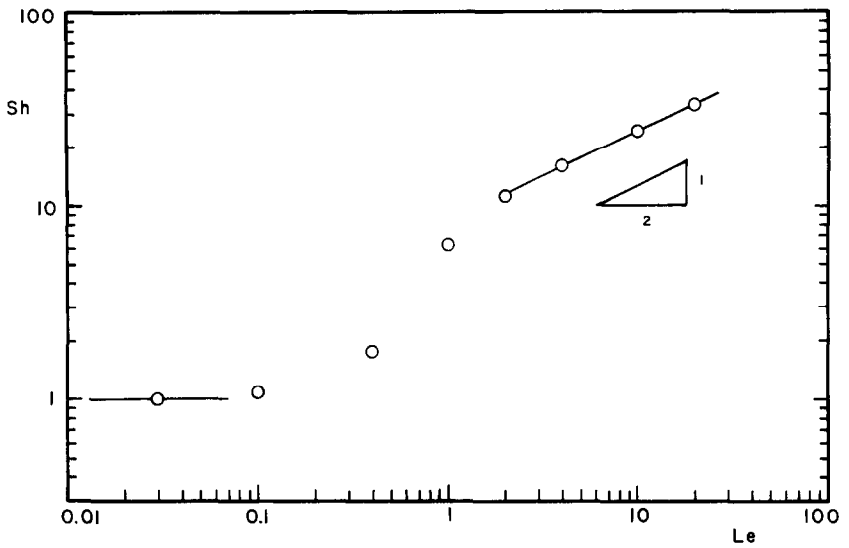

FIG. 7. The transition to the pure mass diffusion regime as the Lewis number decreases ($n = 0$, $Ra = 10^3$, $H/L = 1$).

Sherwood number results for the heat-transfer-driven boundary-layer regime ($n = 0$, large Ra) in vertical porous layers subjected to three sets of side conditions:

i. constant temperature and concentration, ref. [5]
ii. constant heat and mass fluxes, Table 2
iii. constant heat flux and constant concentration, i.e. *mixed* boundary conditions, Table 7.

The Rayleigh number Ra plotted on the abscissa in Fig. 9 is based on heat flux, equation (34). Therefore, in order to plot the data of ref. [5] on Fig. 9 we first converted the ΔT-based Rayleigh number of ref. [5] into the Rayleigh number Ra defined by equation (34): the conversion formula is

$$Ra_{\Delta T,\text{ref.}[5]} = Ra/Nu_{\text{ref.}[5]} \tag{56}$$

where, for the data of ref. [5] only, Ra is based on the wall averaged heat flux $\bar{q}'' = \int_0^1 q''\,\mathrm{d}\hat{y}$.

It is clear from Fig. 9 that the specification of how the heat and mass transfer effects are distributed along the vertical side walls of the porous layer has only a minor impact on overall quantities such as Sh. This conclusion is important because, given the success of the Oseen-linearized solution in predicting the numerical results corresponding to constant heat and mass flux from the side, it means that the same solution can be used to approximate the overall heat and mass transfer rates in cases where the side conditions depart from the constant q'' and j'' model. In those cases, however, one must be careful to interpret the Rayleigh number Ra of equations (33) and (34) as the Rayleigh number based on height-averaged heat flux.

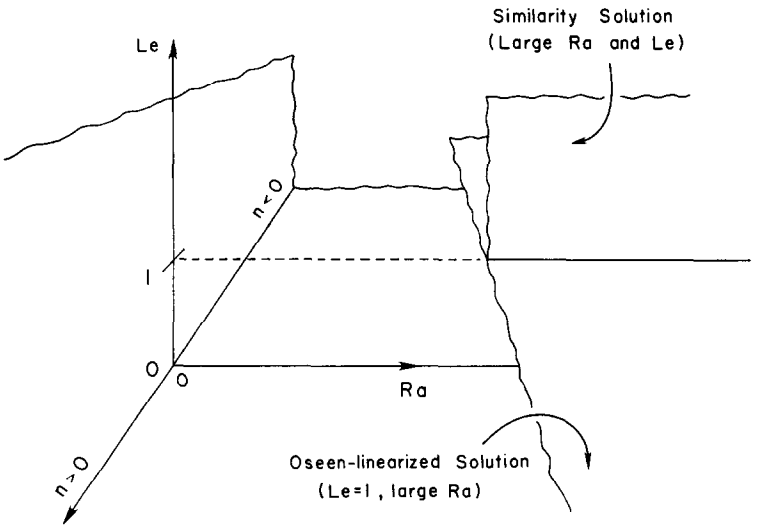

FIG. 8. The (Ra, n, Le) domain for natural convection heat and mass transfer in a porous layer with fixed aspect ratio H/L.

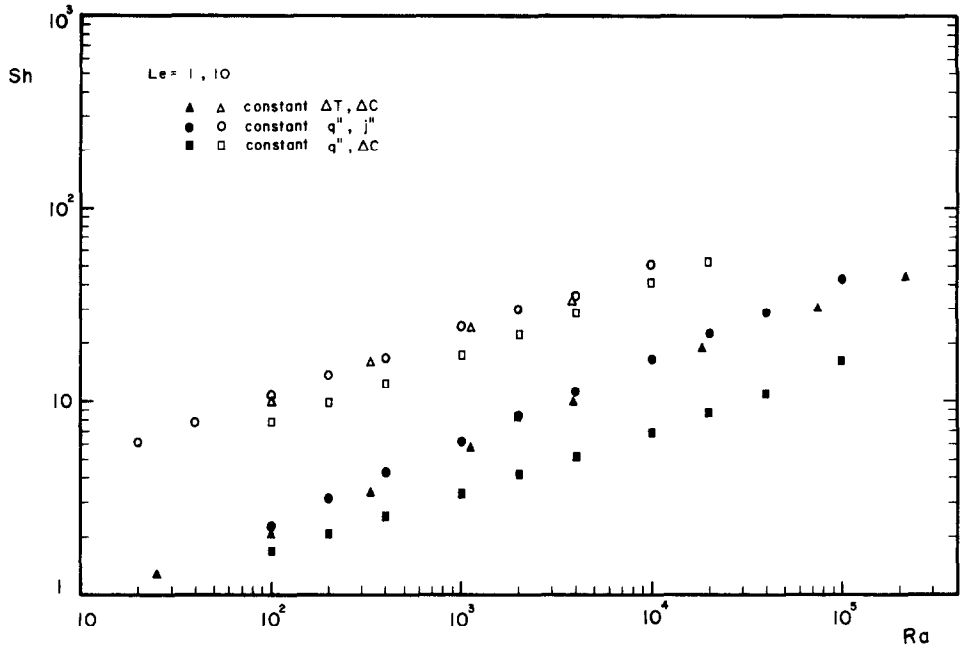

FIG. 9. The effect of boundary conditions on the overall mass transfer rate through a porous layer in the heat-transfer-driven boundary layer regime ($n = 0$, $H/L = 1$).

CONCLUDING REMARKS

In order to describe the potential for heat and mass transfer associated with the natural circulation through a vertical porous layer, we have developed two analytical solutions and an extensive set of numerical simulations designed to cover the parametric domain in which the natural convection phenomenon can exist. The Oseen-linearized solution that yielded the overall heat and mass transfer correlation (33) was developed for porous media with $Le = 1$ and a buoyancy effect ruled by both temperature and concentration variations (finite n), in the high Rayleigh number regime where the heat and mass transfer rates differ greatly from estimates based on the assumption of pure diffusion. The similarity solution that produced the overall mass transfer result (44) was developed for an entirely different limit of the ($Ra, n, Le, H/L$) parametric domain, namely, the class of heat-transfer-driven flows with concentration boundary layers that are thinner than the thermal and velocity boundary layers ($n = 0$, $Le > 1$).

The parametric domain covered by the present theory and numerical experiments is shown in Fig. 8. A comparison with an earlier numerical study [5] of convection driven by constant ΔT and ΔC, Fig. 9, indicates that—properly transformed—the present theoretical results can be used to anticipate the numerical results of ref. [5].

Table 7. Numerical results for heat-transfer-driven natural convection in a porous layer with mixed boundary conditions, constant q'' and constant ΔC along the vertical sides ($n = 0$, $H/L = 1$, grid fineness 32×32, $s = 4$ unless specified in parentheses)

		Sh for *Le* =				
Ra	*Nu*	0.1	0.3	1	3	10
100	2.29	1.00	1.06($s = 1$)	1.69	3.86($s = 1$)	7.79
200	3.05			2.07		9.83
400	4.10			2.55		12.44
1000	6.11	1.04	1.34($s = 1$)	3.37	8.61($s = 2$)	17.17
2000	8.28			4.17		22.16
4000	11.20			5.17		28.78
10,000	16.61	1.15	2.11	6.88	18.73	40.72
20,000	22.26			8.60		52.69
40,000	29.60			10.96		
100,000	42.46			16.03		

Acknowledgements—Visiting Professor O. V. Trevisan wishes to acknowledge the support received from his home institution, Universidade Estadual de Campinas, Brasil. Both authors wish to thank the University of Colorado and Professor M. C. Branch for their hospitality and support of the computational work.

REFERENCES

1. P. Cheng, Heat transfer in geothermal systems, *Adv. Heat Transfer* **14**, 1–105 (1979).
2. A. Bejan, *Convection Heat Transfer*, Chaps 10, 11. Wiley, New York (1984).
3. P. Cheng, Geothermal heat transfer. In *Handbook of Heat Transfer*, (Edited by W. M. Rohsenow, J. P. Hartnett and E. Ganic), 2nd edn. McGraw-Hill, New York (1985).
4. A. Bejan, *Convection Heat Transfer*, pp. 335–338. Wiley, New York (1984).
5. O. V. Trevisan and A. Bejan, Natural convection with combined heat and mass transfer buoyancy effects in a porous medium, *Int. J. Heat Mass Transfer* **28**, 1597–1611 (1985).
6. A. Bejan, The boundary layer regime in a porous layer with uniform heat flux from the side, *Int. J. Heat Mass Transfer* **26**, 1339–1346 (1983).
7. S. Patankar, *Numerical Heat Transfer and Fluid Flow*. Hemisphere, New York (1980).

TRANSFERT DE CHALEUR ET DE MASSE PAR CONVECTION NATURELLE DANS UNE COUCHE VERTICALE DE MILIEU POREUX

Résumé—On étudie analytiquement et numériquement la convection naturelle de chaleur et de masse à travers une couche poreuse verticale soumise à des flux uniformes de chaleur et de masse sur un coté. L'écoulement est conduit par l'effet combiné d'Archimède dû aux variations de température et de concentration à travers le milieu poreux. La première partie de l'étude contient une solution analytique linéarisée d'Oseen pour le régime de couche limite à $Le = 1$, et une solution de similitude pour des écoulements conduits par le transfert de chaleur ($n = 0$) et avec $Le < 1$. La seconde partie de l'étude contient une suite d'expériences numériques qui valide les résultats analytiques et fournit des données dans le domaine non couvert par l'analyse. Les résultats numériques s'étendent dans le domaine de nombre de Rayleigh $20 < Ra < 10^5$, celui du rapport de gravité $-11 < n < 9$, celui du rapport de forme $1 < H/L < 4$ et celui du nombre de Lewis $0{,}03 < Le < 40$.

WÄRME- UND STOFFTRANSPORT BEI NATÜRLICHER KONVEKTION IN EINEM VERTIKALEN PORÖSEN SPALT

Zusammenfassung—Der Wärme- und Stofftransport bei natürlicher Konvektion durch eine vertikale poröse Schicht wird analytisch und numerisch untersucht, wobei von der Seite her ein gleichförmiger Wärme- und Stoffstrom aufgezwungen ist. Die Strömung wird durch Auftriebseffekte aufrechterhalten, die aufgrund von Temperatur- und Konzentrationsunterschieden im porösen Medium auftreten. Im ersten Teil der Arbeit wird eine analytische, nach Oseen linearisierte Lösung für das Grenzschichtgebiet und $Le = 1$ vorgestellt, außerdem eine Ähnlichkeitslösung für die durch Wärmetransport verursachten Strömungen ($n = 0$) und $Le > 1$. Der zweite Teil der Arbeit umfaßt umfangreiche numerische Experimente, welche die analytischen Befunde bestätigen und Daten für den Wärme- und Stofftransport in dem Bereich liefern, der nicht von der analytischen Lösung abgedeckt ist. Die numerischen Ergebnisse umfassen folgende Bereiche: Rayleigh-Zahl $20 \leqslant Ra < 10^5$, Auftriebskennzahl $-11 < n < 9$, Verhältnis der Abmessungen $1 < H/L < 4$ und Lewis-Zahl $0{,}03 < Le < 40$.

СВОБОДНОКОНВЕКТИВНЫЙ ТЕПЛО-И МАССОПЕРЕНОС В ВЕРТИКАЛЬНОЙ ЩЕЛИ, ЗАПОЛНЕННОЙ ПОРИСТОЙ СРЕДОЙ

Аннотация—Аналитически и численно изучается свободноконвективный тепло-и массообмен через вертикальный пористый слой, к поверхности которого подводятся однородные потоки тепла и массы. Течение вызывается подъемной силой, обусловленной как изменениями температуры, так и концентрации по всей пористой среде. В первой части работы представлено аналитическое линеаризованное по Озеену решение уравнения в приближении пограничного слоя с $Le = 1$, а также автомодельное решение для течений, вызванных неоднородностями температуры ($n = 0$) и $Le > 1$. Во второй части приведены данные численных экспериментов, которые подтверждают аналитические результаты по тепло-и массообмену в области параметров вне аналитического решения. Численные результаты охватывают диапазоны: чисел Рэлея $20 \leq Ra \leq 10^5$, коэффициента плавучести $-11 \leq n \leq 9$, геометрического отношения сторон $1 \leq H/L \leq 4$ и числа Льюиса $0{,}03 \leq Le$.